Materials Research Proceedings 41 (2024) 2429-2436 https://doi.org/10.21741/9781644903131-267

# Cellular automata and crystal plasticity modelling for metal additive manufacturing

KAVOUSI Majid[1,a*], MCGARRY Patrick[2,b], MCHUGH Peter[2,c] and LEEN Seán[1,d]

[1]Mechanical Engineering, School of Engineering, University of Galway, Galway, Ireland

[2]Biomedical Engineering, School of Engineering, University of Galway, Galway, Ireland

[a]m.kavousi1@universityofgalway.ie, [b]patrick.mcgarry@universityofgalway.ie, [c]peter.mchugh@universityofgalway.ie, [d]sean.leen@universityofgalway.ie

**Keywords:** Additive Manufacturing, Cellular Automaton, Crystal Plasticity

**Abstract.** This paper presents a methodology to establish a process-structure-property (PSP) relationship for the additive manufacturing (AM) of small AISI 316L parts, as might be used in coronary stent applications. The methodology includes a physically based process-structure model based on cellular automata (CA) for microstructure characterization and generation, coupled with crystal plasticity finite element (CPFE) structure-property modelling to predict the mechanical response of the AM part under tensile loading. The effect of AM process variables, such as laser power and scanning speed, are reflected in the PSP modelling through the thermal modelling of AM feeding into the CA model. The CA method is shown to be able to capture microstructure texture, which is key to anisotropic behavior of AM parts. The present study aims to (i) establish a practical link between CA and CPFE models and (ii) identify optimal process variables with respect to ductility.

## Introduction

Metal additive manufacturing (AM) is revolutionizing the manufacturing industry through a layer-by-layer built process, enabling highly complex, bespoke, and customizable designs, especially in biomedical application. However, the characteristic microstructures resulting from metal AM processes, including grain morphologies and texture distributions, as well as void distributions, for example, are quite different from those of more conventional manufacturing processes. These AM-induced microstructures and defects in turn have a strong influence on resulting mechanical behavior. This can lead to undesirable and hard-to-predict mechanical properties [1].

The texture associated with AM parts and the build direction have been shown to result in orientation-dependent and anisotropic mechanical properties, such as ductility and tensile strength [2,3]. This may be attributed to the directional and high cooling rates in powder bed fusion (PBF) and the epitaxial and directional solidification of cubic crystals (such as FCC for 316L stainless steel).

It is difficult to predict the relationships between process variables and the mechanical response of the printed part or to design the process to achieve specific mechanical performance. Computational simulation is a possible methodology to help understand these relationships and thus the micro-mechanical characteristics of metal AM parts.

The present work is focused on development of a physically based process-structure-property (PSP) methodology for powder bed fusion (PBF), to provide a better understanding of the effects of process variables, and hence facilitate improved process design to avoid detrimental defects and achieve specific mechanical response.

In this study, a cellular automata (CA) process-structure model, for simulation of AM-induced microstructure for thin stainless-steel members [4], is sequentially coupled with a crystal plasticity

Content from this work may be used under the terms of the Creative Commons Attribution 3.0 license. Any further distribution of this work must maintain attribution to the author(s) and the title of the work, journal citation and DOI. Published under license by Materials Research Forum LLC.

finite element (CPFE) structure-property model to predict mechanical response of the synthetically-generated CA microstructure-sensitive models under tensile loading.

**Methodology**

*Cellular automata solidification growth model*

A single dendrite with a face-centered cubic (fcc) lattice structure is shown to grow with an octahedral grain morphology in an undercooled melt, in both experiments [5] and simulations [6]. <100> directions represent the half diagonals of the octahedron. All the diagonals of the octahedron are of the same length under uniform thermal conditions as shown in Fig. 1 (a). For a 2D representation of the growth envelope, one of the <100> directions of the grain is assumed to be normal to the 2D simulation plane (Fig. 1 (b))

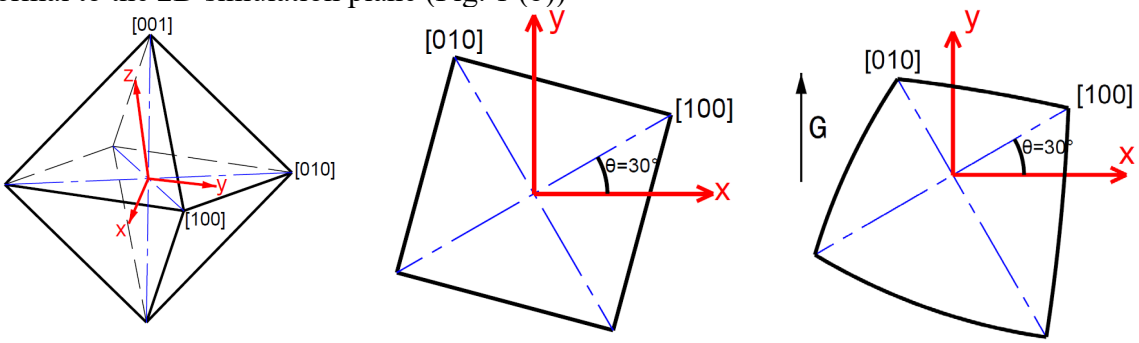


(a) (b) (c)

*Fig. 1 The growth envelope under uniform thermal conditions in (a) 3D and (b) 2D, (c) thermal gradient in y direction in 2D.*

The basic cellular automata (CA) algorithm for modelling solidification growth is described in terms of the growth of a single nucleus in a melt pool with uniform temperature distribution. The physical and thermal parameters are the same as those used in [7]. A rectangular domain of size $L_x \times L_y$ is assumed in the $x$-$y$ plane. The domain is divided into a grid of square cells of size $\Delta x$, resulting in $n_x$ and $n_y$ cells in the $x$ and $y$ directions, respectively. $T_{ij}$ denotes the temperature of cell $ij$ where $i \in \{1, \dots, n_y\}$ and $j \in \{i, \dots, n_x\}$. The undercooling is defined as:

$$\Delta T = T_{liq} - T_{ij} \tag{1}$$

where $T_{liq}$ is liquidus temperature. The initial state of the cells is set as liquid. An initial undercooling of 2K is assigned to all cells to initiate the growth of the nuclei [7]. A nucleus is assumed to be developed from the centre of cell $\eta$. The initial shape of the grain in 2D is a square where the [100] direction is rotated by an angle $\theta$ about the $x$-axis. The square engulfs the dendrite main trunks and arms. The size of the square depends on speed of the dendrite tip, $v_{tip}$, which itself is a function of local undercooling, $\Delta T$. The following relationship is proposed by Kurz et al. [8] between $v_{tip}$ and $\Delta T$:

$$v_{tip} = A(\Delta T)^2 \tag{2}$$

where $A$ is a material dependent constant. The half size of the growth square of the nucleus centered on cell $\eta$ (see Fig. 2 (a)) at time $t$ can be calculated from Eq. (3) or Eq. (4), as below:

$$L_\eta^t = \frac{1}{\sqrt{2}} \int_{t_0}^{t} v\left[\Delta T_\eta(\tau)\right].d\tau \tag{3}$$

$$L_\eta^t = \frac{1}{\sqrt{2}} \sum_{\tau=t_0}^{t} v\left[\Delta T_\eta(\tau)\right] \cdot \Delta\tau \tag{4}$$

New cells are captured as soon as their centre is engulfed by a growth square. The time increment at which four neighbors of cell $\eta$, one highlighted as cell $\mu$ for further explanation, are captured as shown in Fig. 2 (b). Once a new cell is captured, it inherits the properties of the parent cell, i.e., the grain identification number (grain ID) and misorientation, and its state changes liquid to solid. So far, the centre of the growth square is fixed at its initial location, and it keeps growing as long as $\Delta T > 0$, resulting into two issues: (i) the growth square becomes so large that it captures cells that should have been captured by other grains, as in Fig. 2 (c), and (ii) failure to take into account the local undercooling as the growth square grows.

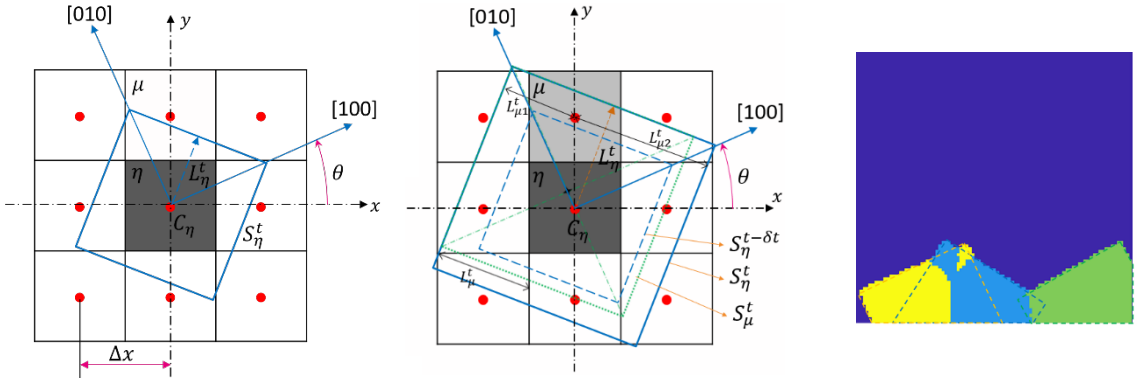


*Fig. 2. The cell capturing mechanism in 2D CA: (a) the growth square, $\boldsymbol{S_\eta^t}$, of the nucleus placed on the centre of cell $\boldsymbol{\eta}$ with a misorientation angle of $\boldsymbol{\theta}$ and its half size, $\boldsymbol{L_\eta^t}$, shown, (b) the time increment at which the cell $\boldsymbol{\mu}$ is captured by the growth square of cell $\boldsymbol{\eta}$. The new truncated decentred growth square for the newly captured cell $\boldsymbol{\mu}$, with is half size of $\boldsymbol{L_\mu^t}$ is shown as well ($\boldsymbol{S_\mu^t}$), and (c) capturing wrong cells by the yellow growth square when it keeps growing.*

To overcome this problem, the decentered square algorithm is introduced. Whenever a new cell is captured, a new growth square is defined for that cell with the following criteria:

1. The new square is fully inside the parent square.
2. A corner of the new square coincides with a corner of the parent square which is closest to the centre of the newly captured cell.
3. The half size of the new square is calculated as below (considering the capture of cell $\mu$ as shown in Fig. 2 (b)):

$$L_\mu^t = \frac{1}{2}\left[\min\left(L_{\mu1}^t, \sqrt{2}\Delta x\right) + \min\left(L_{\mu2}^t, \sqrt{2}\Delta x\right)\right] \tag{5}$$

where $L_{\mu1}^t$ and $L_{\mu2}^t$ are the distances of centre of cell $\mu$ from the two opposite faces of the parent square along the capturing face (the face that has captured cell $\mu$). The growth squares of cell $\eta$ at times $t$ and $t - \delta t$, and the growth square of the captured cell μ are shown in Fig. 2(b) as $S_\eta^t$, $S_\eta^{t-\delta t}$, and $S_\mu^t$, respectively. The newly defined growth squares will grow similarly in each time increment, except with the undercooling associated with their own cell. Once all cells in the Moore neighborhood [9] of a cell are captured, its growth square is deactivated. In the case that multiple squares try to capture a particular cell at the same time step, the first capture in the iteration order

takes precedence. In some cases, the square of the captured cell completely overlaps with the parent square; in such cases, the new square is deactivated for computational efficiency.

*Grain growth algorithm validation*

The CA model for the decentered square grain growth algorithm is validated against the analytical model [10] which, in turn, was validated against experiments [11]. A 10 mm × 10 mm square domain is considered with a cell size of $\Delta x = 5 \times 10^{-5}$ m resulting in $4 \times 10^4$ cells. A nucleus is placed on the cell in the centre of the domain with a misorientation angle of $\theta = 30°$. Three different thermal conditions are defined based on the work of Gandin et al. [10], including spatially isothermal cooling, static thermal field, and Bridgman condition with a fourth condition as static temperature for comparison, as listed in Table 1. A cooling rate of $\dot{T} = -0.1\ \mathrm{Ks^{-1}}$ and a thermal gradient of $G = 250\ \mathrm{Km^{-1}}$ in the Y-direction is used where needed. For all cases, the initial undercooling is 2K, and the time increment is 0.01s.

*Table 1. Different modes of thermal conditions for the simulation of growth of a single nucleus using decentered square algorithm.*

| Mode 1: Spatially isothermal cooling | Mode 2: Static thermal field | Mode 3: Bridgman condition | Mode 4: Static temperature |
|---|---|---|---|
| $G = 0.0\ \mathrm{Km^{-1}}$ | $G = 250\ \mathrm{Km^{-1}}$(Y dir.) | $G = 250\ \mathrm{Km^{-1}}$(Y dir.) | $G = 0.0\ \mathrm{Km^{-1}}$ |
| $\dot{T} = -0.1\ \mathrm{Ks^{-1}}$ | $\dot{T} = 0.0\ \mathrm{Ks^{-1}}$ | $\dot{T} = -0.1\ \mathrm{Ks^{-1}}$ | $\dot{T} = 0.0\ \mathrm{Ks^{-1}}$ |

The evolution of the grain boundary in the CA decentered square algorithm is visualized with 1 s time intervals for all thermal modes listed in Table 1 in Fig. 3 (a-d). The first three modes match perfectly with the analytical results [10], while the fourth mode is also a consistent result. For spatially isothermal cooling, the grain grows uniformly, and the growth rate increases over time as the undercooling increases (see Fig. 3(a)). The static thermal field and Bridgman condition resulted in non-uniform grain growth induced by the thermal gradient, $G$, where grains grow faster in the Bridgman condition because of the presence of cooling rate, $\dot{T}$, as in Fig. 3(b,c). The static temperature mode, on the other hand, produces uniform grain growth with constant growth rate (i.e., equally spaced grain boundaries in 1 s time intervals) as the only reason of grain growth in the initial undercooling (see Fig. 3(d)). The decentered square CA algorithm is developed using MATLAB.

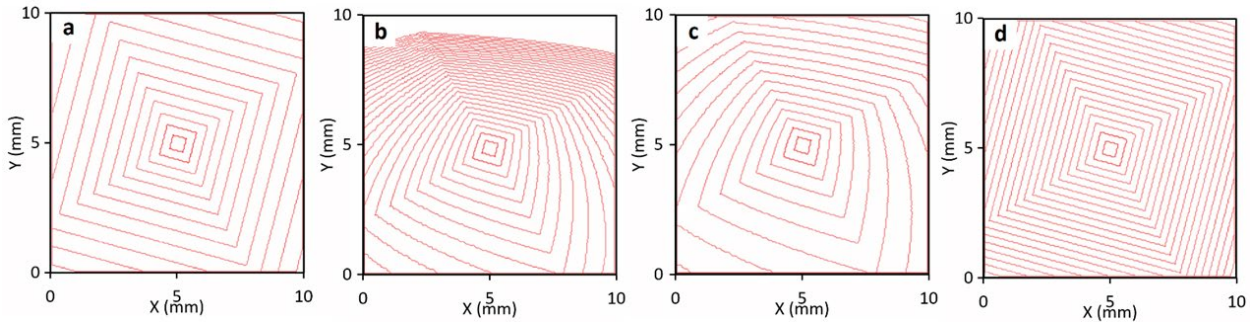


*Fig. 3. The grain boundary of the growing grain associated with the single nucleus on the centre of the domain plotted at 1 s time intervals for different thermal conditions: (a) spatially isothermal cooling, (b) static thermal field, (c) Bridgman condition, and (d) static temperature.*

To model the micro-mechanical behaviour of individual grains of 316L austenitic stainless steel, with a face-centered-cubic (FCC) crystal microstructure and 12 slip systems, single crystal plasticity theory was employed, based on the work of Hill [12], Rice [13], and Asaro [14]. This constitutive behavior has been implemented in a user-defined material (UMAT) for Abaqus [15,16] and is adopted here. More detailed description of the constitutive model is given in our previous work [4].

**Results and discussion**

The proposed CA model when combined with the thermal histories of PBF for metal can produce microstructures that represent AM parts. As a preliminary study, a rectangular model representing a single track-like laser scan, with a thermal gradient in the *y* direction, is modelled, as depicted in Fig. 4(a) with grains y-color map according to the IPF color key. It is apparent from the model that the grains with <100> crystallographic orientations almost parallel to the *y*-axis (build direction) tend to grow faster and eliminate neighboring grains that are not suitable for fast growth (grains with green colors or with <101> direction parallel to the *y*-axis).

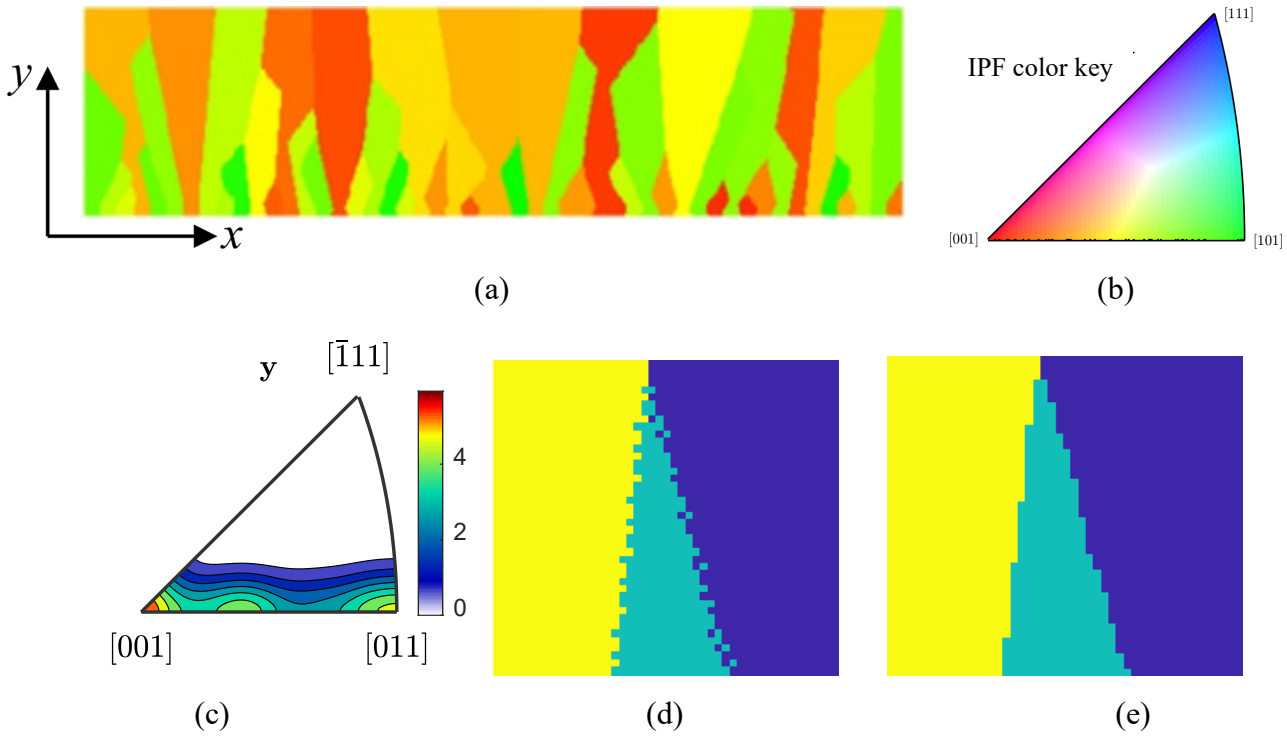


*Fig. 4. CA microstructure model: (a) a sample CA microstructure with grains colored (in direction) according to (b) IPF color key, (c) jagged grain boundaries in a three grain CA growth model, and (d) the grain boundaries after smoothing.*

*CA model optimization for meshing*

In a multi-grain CA model, the grain boundaries may exhibit artificial (synthetic) roughness, as illustrated in Fig. 4(d) for the case of three grains. To mitigate this artifice, a smoothing algorithm is employed to refine the grain boundaries. To achieve this, the grain identification number assigned to each cell is compared with the numbers attributed to the majority of its neighboring cells and changed accordingly. This process eliminates isolated cells and effectively smoothens the jagged grain boundaries, as depicted in Fig. 4(e).

As part of the process-structure-property methodology, the CA microstructure should be converted into a suitable mesh for crystal plasticity finite element (CPFE) analysis. The pixels or cells (voxels in 3D) in the CA model can be converted into regular quadrilateral (hexahedral in

3D) elements. However, this has two main drawbacks: (i) stepped grain boundaries (GBs) which are not appropriate for simulating phenomena like GB sliding, and (ii) a large number of elements due to the relatively small cell size required for CA growth modelling [17]. Alternatively, the CA microstructure model can be meshed using 2D triangular (or 3D tetrahedral) elements within the MATLAB code. For this purpose, GBs in the CA model are extracted for all grains (see Fig. 5(a)). Then, for each grain, the initial GB is rearranged to represent the correct connectivity order, creating a polygon for each grain. This polygon can be meshed straight away. But, since the GB polygons are comprised of the cell edges, the issue with the stepped grain boundaries persists and results in non-uniform mesh distribution with very small elements near the GBs as depicted in Fig. 5(b). To rectify this problem, a Ramer-Douglas-Peucker (RDP) algorithm [18,19] is utilized to simplify the GBs. The triple points for each grain are used as the initial points to start the RDP algorithm. Fig. 5(c) shows the simplified GBs along with the initial ones for the same 10 grain CA microstructure model shown in Fig. 5(c). The significant improvement of the mesh quality using the simplified GBs as input is evident, not only near the GBs but also inside the grain, as illustrated in Fig. 5(d).

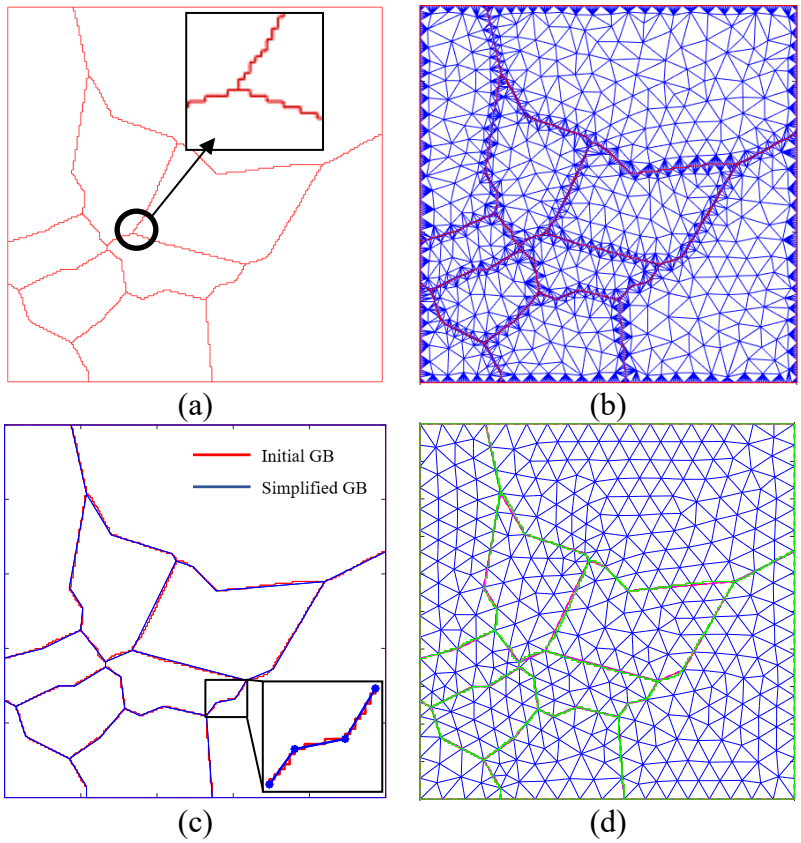


*Fig. 5. CA model optimization for FE meshing: (a) the initial grain boundaries (GB) of a CA model with 10 grains with a portion magnified to show the stepped grain boundaries, (b) the non-uniform mesh generated using the initial GBs with very small mesh close to GBs, (c) the simplified GBs using the RDP algorithm, and (d) the generated mesh using the simplified GBs.*

*CPFE tensile analysis of CA model*

A tensile macroscopic strain of up to 50% has been applied to the microstructure produced with the CA model as shown Fig. 4(a) and the tensile response is analyzed using the CPFE material model. The strain contour plot of the deformed microstructure is depicted in Fig. 6. The FE model is constrained from the two ends and the upper and lower sides are unconstrained, mimicking miniscule components such as cardiovascular stent struts, resulting in free deformation along the

length of the model. Due to heterogeneity of crystallographic orientation, the deformation is also non-uniform (heterogeneous) with regions of localized strains and macroscopic shear band aligned at 45° of the tensile direction.

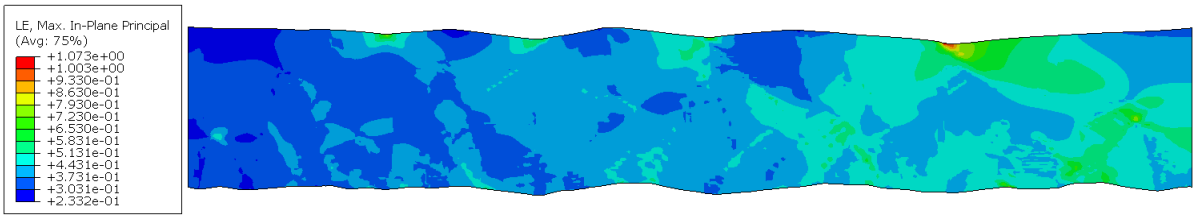


*Fig. 6. The CPFE strain contour plot of the CA microstructure model under 50% macroscopic tensile deformation.*

## Conclusion

A cellular automata process-structure methodology for grain growth was developed, simulating dendritic growth under different thermal conditions – suitable for PBF microstructure morphology and texture modelling; this was linked to CPFE for tensile structure-property simulation, with 50% macroscopic elongation applied to the CA-CPFE model, revealing localized deformation and shear bands. Future and ongoing work includes CA-CPFE sensitivity studies to understand process variable effects on AM part performance, continuing our recent work on PSP modelling of AM 316L struts.

## Acknowledgements

This publication has emanated from research conducted with the financial support of University of Galway Hardiman PhD Scholarship (M. Kavousi) and Science Foundation Ireland under Grant number SFI/16/RC/3872. For the purpose of Open Access, the author has applied a CC BY public copyright license to any Author Accepted Manuscript version arising from this submission.

## References

[1] T. Ronneberg, C.M. Davies, P.A. Hooper, Revealing relationships between porosity, microstructure and mechanical properties of laser powder bed fusion 316L stainless steel through heat treatment, Mater. Des. 189 (2020). https://doi.org/10.1016/j.matdes.2020.108481

[2] X. Yang, X. Wang, M. Brochu, X. Wang, N.M. Harrison, S.B. Leen, J. Segurado, Understanding orientation-dependent plasticity in laser beam powder bed fusion stainless steel through crystal plasticity modelling, Mater. Sci. Eng. A 852, (2022). https://doi.org/10.1016/j.msea.2022.143682

[3] X. Wang, J.A. Muñiz-Lerma, O. Sánchez-Mata, M.A. Shandiz, M. Brochu, Microstructure and mechanical properties of stainless steel 316L vertical struts manufactured by laser powder bed fusion process, Mater. Sci. Eng. A 736, (2018) 27–40. https://doi.org/10.1016/j.msea.2018.08.069

[4] M. Kavousi, P. McGarry, P. McHugh, S. Leen, Geometrical and crystal plasticity modelling: Towards the establishment of a process-structure-property relationship for additively manufactured 316L struts, Eur J Mech A Solids 102 (2023). https://doi.org/10.1016/j.euromechsol.2023.105115

[5] D.E. Ovsienko, G. A. Alfintsev, Crystal Growth from the Melt Experimental Investigation of Kinetics and Morphology, *Crystals: growth and properties. Berlin: Springer-Verlag* (1980): 119-70.

[6] G. I. Tóth, G. Tegze, T. Pusztai, G. Tóth, L. Gránásy, Polymorphism, crystal nucleation and growth in the phase-field crystal model in 2D and 3D, J. Phys. Condens. Matter 22 (2010). https://doi.org/10.1088/0953-8984/22/36/364101

[7] C.A. Gandin, M. Rappaz, A 3D cellular automaton algorithm for the prediction of dendritic grain growth, Acta Mater. 45 (1997) 2187-2195. https://doi.org/10.1016/S1359-6454(96)00303-5

[8] W. Kurz, B. Giovanola, R. Trivedi, Theory of microstructural development during rapid solidification, Acta metall. 34 (1986) 823–830. https://doi.org/10.1016/0001-6160(86)90056-8
[9] D.A. Zaitsev, A generalized neighborhood for cellular automata, Theor Comput Sci 666 (2017) 21–35. https://doi.org/10.1016/j.tcs.2016.11.002
[10] C.A. Gandin, R.J. Schaefer, M. Rappaz, Analytical and numerical predictions of dendritic grain envelopes, Acta mater. 44.8 (1996) 3339-3347. https://doi.org/10.1016/1359-6454(95)00433-5
[11] D.E. Ovsienko, G.A. Alfintsev, V.V. Maslov, Kinetics and shape of crystal growth from the melt for substances with low L/kT values, J. Cryst. Growth 26 (1974) 233-238. https://doi.org/10.1016/0022-0248(74)90251-6
[12] R. Hill, Generalized constitutive relations for incremental deformation of metal crystals by multislip, J. Mech. Phys. Solids 14 (1966) 95–102. https://doi.org/10.1016/0022-5096(66)90040-8
[13] J.R. Rice, Inelastic constitutive relations for solids : an internal-variable theory and its application to metal plasticity, J. Mech. Phys. Solids 19 (1971) 433–455. https://doi.org/10.1016/0022-5096(71)90010-X
[14] R.J. Asaro, Micro Mechanics of Crystals and Polycrystals, Adv. Appl. Mech. 23 (1983) 1-115. https://doi.org/10.1016/S0065-2156(08)70242-4
[15] Y. Huang, A user-material subroutine incroporating single crystal plasticity in the ABAQUS finite element program. Harvard Univ. Cambridge, MA, 1991.
[16] J. W. Kysar and P. Hall, Addendum to a User-material Subroutine Incorporating Single Crystal Plasticity in the ABAQUS Finite Element Program: Mech Report 178., Cambridge, 1997.
[17] J. Segurado, R.A. Lebensohn, J. Llorca, Computational Homogenization of Polycrystals, Adv. Appl. Mech. 51 (2018) 1–114. https://doi.org/10.1016/bs.aams.2018.07.001
[18] D.H. Douglas T.K. Peucker, Algorithms for the reduction of the number of points required to represent a digitized line or its caricature, Int J Geogr Inf Sci 10 (1973) 112–122. https://doi.org/10.3138/FM57-6770-U75U-7727
[19] U. Ramer, An Iterative Procedure for the Polygonal Approximation of Plane Curves, Comput. graph. image process 1 (1972) 244–256. https://doi.org/10.1016/S0146-664X(72)80017-0